Article

Thermal analysis of a fast charging technique for a high power lithium ion cell.

V.M. García [1]* , C. Blanco [2], D. Anseán [2], M. González [2], Y. Fernández Pulido [2] and J. C. Antón [2]

[1] University of Oviedo, Department of Physical and Analytical Chemistry, Campus de Gijón, Edificio Polivalente, 33204 Gijón, Asturias, Spain

[2] University of Oviedo, Department of Electrical Engineering, Campus de Gijón, Módulo 3, 33204 Gijón, Asturias, Spain

* Correspondence: victorg@uniovi.es (Víctor M. García); Tel.: +34 985 182 2268

Abstract: The cell case temperature versus time profiles of a multistage fast charging technique (4C-1C-CV)/fast discharge (4C) in a 2.3 Ah cylindrical lithium-ion cell are analyzed using a 1D thermal model. Heat generation is dominated by the irreversible component associated to cell overpotential, although evidences of the reversible component are also observed, associated to the heat related to entropy from the electrode reactions. The final charging stages (i.e., 1C-CV) significantly reduce heat generation and cell temperature during charge, resulting in a thermally safe charging protocol. Cell heat capacity was determined from cell specific heats and cell materials thickness. The 1D model adjustment of the experimental data during the 2 min. resting period between discharge and charge allowed us to calculate both the time constant of the relaxation process and the cell thermal resistance. The obtained values of these thermal parameters used in the proposed model are almost equal to those found in the literature for the same cell model, which suggests that the proposed model is suitable for its implementation in thermal management systems.

Keywords: thermal model ; fast charge ; lithium-ion cell.

1. Introduction

In recent years, battery fast charging has become a thriving area of research, as a result of the increasing demands in portable electronics [1], electric vehicles [2] and electrical energy storage systems [3]. Despite its convenience, battery fast charging can drastically reduce cell longevity if improperly addressed. This is primarily caused by the elevated cell temperatures and high currents used during fast charging, which are identified as the two main factors that accelerate battery degradation [4] and reduce battery state-of-safety [5].

Even so, battery fast charging capabilities can be enhanced by modifying cell active materials and cell design [6], and improving the charging algorithm [7] ,[8]. In addition, the effect of battery heat generation plays also a major role for fast charging [9]. Hence, a detailed battery thermal analysis during fast charging could be used to design safer, quicker and more efficient charging protocols.

In this work, we propose a 1D thermal model to decipher the heat generation contributions (both reversible and irreversible) during battery fast charging. The battery fast charging

technique thermally studied here was previously reported in [10], and was validated to attain quick recharges while causing no accelerated cell degradation [11]. The proposed 1D thermal model is similar to several thermal models found in the literature [12] [13] [14] [15], but it presents a low-computational complexity, and utilizes external cell surface temperature as the main variable to infer heat generation during operation. Despite using a similar approach as presented here, other models [16] present more complex, higher order differential equations which could be more difficult to implement in commercial battery management systems (BMS).

The findings from this work improves the understanding of the thermal behavior of this particular fast charging technique, while using a simple, effective thermal model.

The paper is organized as follows: Section 2 presents the main features of the fast charging method as well as the measurements made to implement the thermal analysis, Section 3 explains the thermal model and Section 4 shows and discusses the obtained results, highlighting how the thermal capacity and the thermal resistance of the cell are obtained. Finally, Section 5 presents the conclusions.

2. Experimental

The experiments were conducted on a comercial Graphite/$LiFePO_4$ (C/LFP) cylindrical cell, manufactured by A123 Systems (ANR26650M1). These cells have a rated capacity of 2.3 Ah and a nominal cell voltage of 3.3 V when evaluated at nominal cell conditions, i.e., 1C rate. The cells have an average weight of 0.075 kg. The specific energy under nominal conditions is about 99.2 Wh kg^{-1} [17]. Cell characterization and cycle aging were conducted using a multi-channel Arbin BT-2000 battery tester. The cell-surface temperature was monitored using T-type thermocouples manufactured by Omega. The thermocouples were attached to the cell surface using self-adhesive thermocouple pads. A Memmert climate chamber was used to maintain constant ambient temperature of 22ºC throughout testing.

The cells were started with the commissioning test, in which they were identified and weighted. Next, a conditioning series was performed following the USABC test procedures [18]. Thereafter, C/25 charge and discharge cycles were carried out to determine a practical maximum capacity with minimal kinetic effects [19], [20]. Subsequently, the cells were subjected to cycling. The cycling scheme consisted in fast charging and fast discharging. Fast charging consisted of a multistage fast charging technique using three charging steps at 4C (9.2A), 1C (2.3A) under constant current, and a fixed 5-min length constant voltage (CV) stage at 3.6 V. Discharges were carried out at 4C (-9.2A) to 2.0 V cut off voltage. After a resting time of 2 minutes the process starts again.

The used multistage fast charging technique profile is shown in Figure 1, showing the evolution of cell voltage, current and temperature (both cell temperature surface and ambient temperature), for three consecutive cycles. More details of this method can be found in our previous work [10].

Peer-reviewed version available at Batteries 2016, 2, 32; doi:10.3390/batteries2040032

This sequence was performed continuously for 300 cycles, after which the reference tests were performed. The test sequence includes two cycles with standard charges at 1 C and discharges at 1 C and C/3, followed by a final constant current charge and discharge cycle at C/25 (0.092 A). The C/25 rate is considered slow enough to obtain a practical approach to the open circuit voltage (OCV) of the cell [21]. If the OCV is represented as a function of the estate of charge, E(SOC), it provides a pseudo-thermodynamic description of the cell voltage with negligible kinetic effects, and it is used as a reference to obtain the resistance of the cell R_{cell}(SOC) during the charge and the discharge. Both resistances are necessary to measure the irreversible component of the heat generation.

Taking into account that charging current is considered positive and discharging current is considered negative, the cell resistance is defined as Equation 1:

$$R_{\text{cell}}(\text{SOC}) = \frac{V(\text{SOC}) - E(\text{SOC})}{I} \quad (1)$$

where V(SOC) is the battery voltage for both charge (V(SOC) > E(SOC)) and discharge (V(SOC) < E(SOC)).

Figure 1 also shows the temperature profile at the casing battery measured by means of a thermocouple. The ambient temperature is 22º C. A repetitive pattern can be observed: the casing temperature varies between 24º C at the end of the charge and 27º C at the end of both 4C charge and discharge stages.

To obtain the average thermal capacity of the cell from the specific density and specific heat of its components the cell has been open in glove box and the thickness of the collectors, separators and electrodes have been measured by means of a micrometer screw.

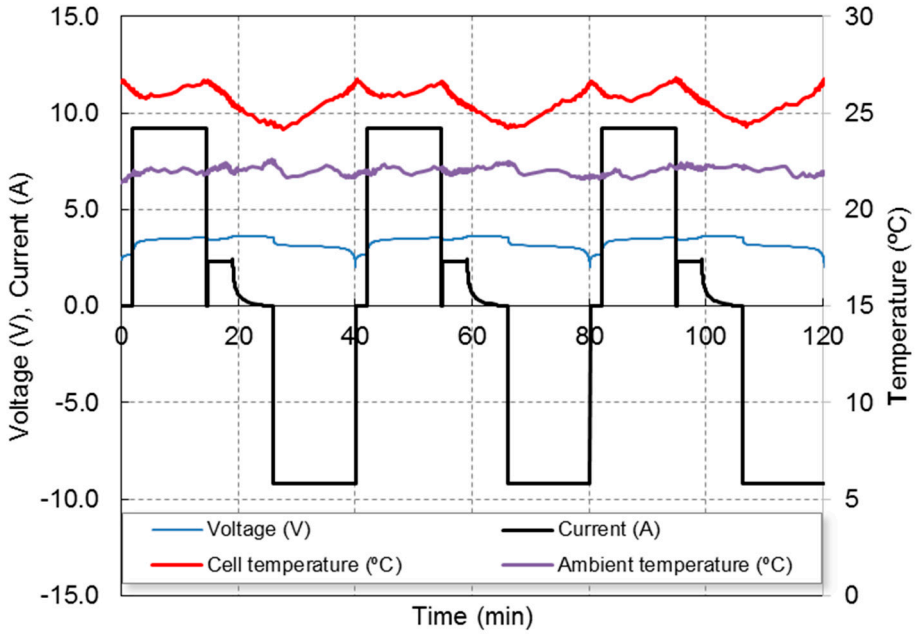

Figure 1. Cell temperature, current and voltage evolution during 4C-1C-CV/4C cycling.

Peer-reviewed version available at Batteries 2016, 2, 32; doi:10.3390/batteries2040032

3. Model

The cell is assumed to be small enough so that it is considered a body with constant thermal capacity, C_{cell} (J/K), and uniform internal temperature T_{int} (K). This temperature will change (Equation 2) as a result of the balance between the stored internal energy, the heat generated (W) by the cell operation and the heat exchanged (W) with the outside environment at constant temperature T_{ext} (K).

$$C_{\text{cell}} \frac{dT_{\text{int}}}{dt} = \dot{Q}_{\text{gen}} + \dot{Q}_{\text{exch}} \quad (2)$$

The exchanged heat (Equation 3) is considered proportional to (a) the total area (lateral and bases), A_{cell} (m^2), of the cell, and (b) the temperature difference between the ambient temperature, T_{ext}, and the battery casing temperature, T (K).

The proportionality constant is the heat transfer coefficient, h_{ext} ($Wm^{-2}K^{-1}$). h_{ext} only depends on convective cooling conditions.

$$\dot{Q}_{\text{exch}} = h_{\text{ext}} A_{\text{cell}} (T_{\text{ext}} - T) \quad (3)$$

Heat generated inside the cell, when a current flows through the cell, has two main components during normal operation. The first is the irreversible heat linked to full overpotential which includes the charge transfer processes of the reactions at the surface of the electrode particles, the mass transport by diffusion to/from the surface, and the voltage drop on the metal parts and the electrolyte. These processes are responsible for the overpotential defined as the difference between the battery voltage (V) when current flows through the battery and quasi-equilibrium voltage of the battery (E). This irreversible heat is defined by Equation 4 for both charge and discharge. It is a exothermic dissipative component ($\dot{Q} > 0$) that heats the cell for both charge and discharge.

$$\dot{Q}_{\text{gen,irrev}} = I(V - E) = I^2 R_{\text{cell}} \quad (4)$$

The heat generated reversibly is linked to entropic change of electrode reactions. Applying basic thermodynamic relationships, the definition of the reversible component is given by Equation 5:

$$\dot{Q}_{\text{gen,rev}} = T \frac{dE}{dT} I \quad (5)$$

where the current is positive for charge and negative for discharge, and the thermal coefficient of the cell is dE/dT for both charge and discharge. If the discharge reaction of the cell is exothermic and warms the cell, the discharge reaction of the cell is endothermic and cools the cell.

A part of the heat generated by the cell is transported first by conduction from the inside the cell, whose temperature is T_{int}, to the outer surface of the cell casing, whose temperature is T, and then from the cell casing to the outside the cell, whose temperature is T_{ext}. This heat flow is expressed by the Equation 6:

$$h_{\text{int}}A_{\text{cell}}(T_{\text{int}} - T) = -h_{\text{ext}}A_{\text{cell}}(T_{\text{ext}} - T) \quad (6)$$

where the internal heat transfer coefficient, h_{int}, is considered an effective amount that absorbs any difference in the thermal conductivities that may exist in the radial direction and the axial direction of the cylindrical cell.

Inverse coefficients h_{int} and h_{ext} are the corresponding thermal resistances $R_{\text{th,int}}$ and $R_{\text{th,ext}}$ respectively. The sum of these two resistances, R_{th} (K/W), is defined by Equation 7:

$$R_{\text{th,int}} = \frac{1}{h_{\text{int}}A_{\text{cell}}}, \quad R_{\text{th,ext}} = \frac{1}{h_{\text{ext}}A_{\text{cell}}}, \quad R_{\text{th}} = R_{\text{th,int}} + R_{\text{th,ext}} \quad (7)$$

Internal temperature (T_{int}), which is not measurable, is eliminated from Equation 2 using Equations 3, 6 and 7. The outer surface of the cell casing, T, and the environment temperature, T_{ext}, appears instead of T_{int}. Both T and T_{ext} are easily measurable. Equation 2 becomes Equation 8:

$$C_{\text{cell}}R_{\text{th}}\frac{dT}{dt} = R_{\text{th,ext}}\dot{Q}_{\text{gen}} + T_{\text{ext}} - T \quad (8)$$

For small cells, this simplified model provides good results with little computational effort. As shown in next section, the obtained values for thermal parameters C_{cell} and R_{th} are almost identical to those obtained with other methods in [15].

4. Results and discussion

The time axis of Figure 1 is transformed into the SOC axis for discussing the temperature profiles. The used relationships have been (Equation 9):

$$\frac{SOC}{100} = \frac{Q_{max} - |I_{\text{dis}}|t}{Q_{max}}, \quad \text{for discharge} \qquad \frac{SOC}{100} = \frac{Q_{max} - I_{\text{ch}}t}{Q_{max}}, \quad \text{for charge} \quad (9)$$

where I_{dis} = -9.2 A for the fast discharge at 4C. For the 4C-1C-CV multistage charging method I_{ch} = 9.2 A for the CC stage at 4C, I_{ch} = 2.3 A for the charge stage at CC stage at 1C and I_{ch} = I(t) for the CV stage. The measured battery capacity at C/25 is taken as the maximum capacity for both charge and discharge: Q_{max} = 2.3 Ah. The discharge capacity at 4C is slightly lower than Q_{max}. The charge capacity using the 4C-1C-CV multistage charging method is almost equal to Q_{max} due to the final CV stage.

Figure 2a shows the measured voltage for the quasi-thermodynamic discharge at C/25, the measured voltage for a fast discharge at 4C, I_{dis} = -9.2 A, and the internal resistance of the cell obtained by applying Equation 1. The value of the internal resistance is about 20 mΩ except near the full discharge area (SOC = 0), where the E(SOC)-V(SOC) polarization is very high. The internal resistance presents intermediate peaks due to there are steps in the voltage curve E(SOC). These voltage steps are caused by staying compounds of the cell graphite [22]. Figure 2b shows the value of the internal resistance for a 4C-1C-CV fast charge cycle. At C/25, charging curve E is slightly higher than discharging curve E due to structural hysteresis [23]. The resistance step near full charge area (SOC = 90) shown in Figure 2b is

Peer-reviewed version available at Batteries 2016, 2, 32; doi:10.3390/batteries2040032

generated by the corresponding step in the 4C-1C-CV multistage charging voltage. The resistance values are lower for charge than for discharge. For charge, the typical value for internal resistance is 15 mΩ, which is according to references [24][25]. Unlike at the end of discharge, polarization $I \cdot R_{cell} = V\text{-}E$ near full charge tends to a very low value because the CV stage ends with a very low current value when $E(SOC) \approx V(SOC)$.

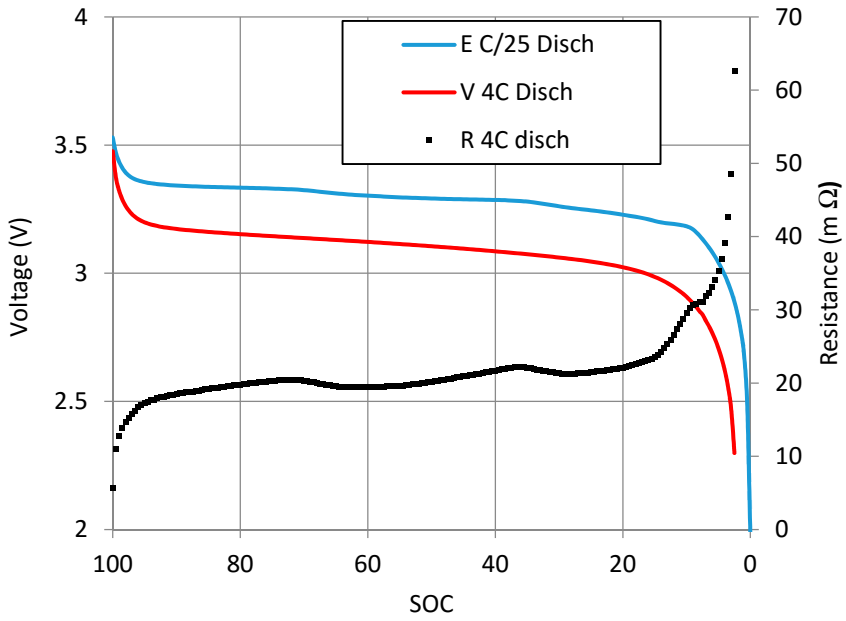

(**a**)

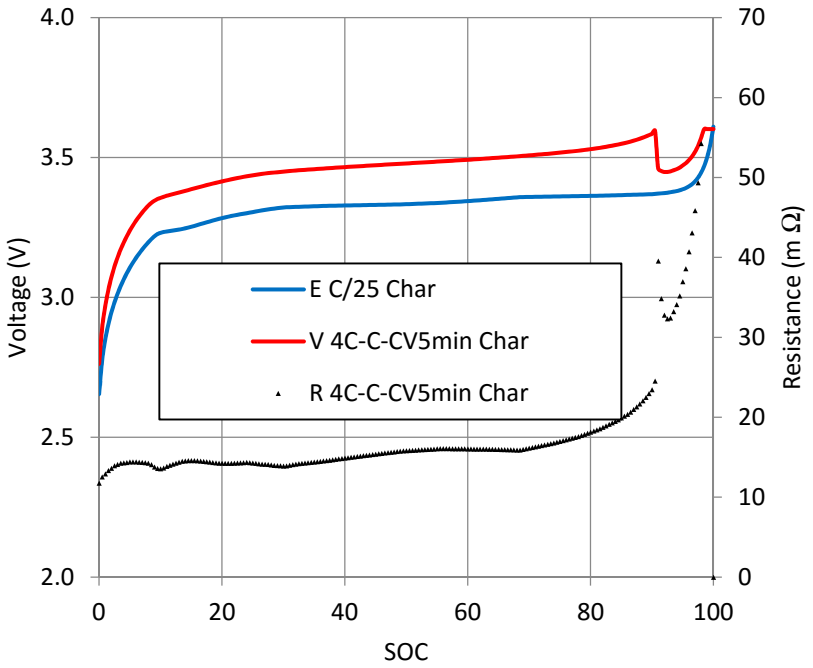

(**b**)

Figure 2. (**a**) Internal resistance evolution profile versus state of charge of the cell, 4C discharge; and (**b**) 4C-1C-CV5min charge.

Peer-reviewed version available at Batteries 2016, 2, 32; doi:10.3390/batteries2040032

The heat generation power is shown in Figure 3a for a 4C discharge and it is shown in Figure 3b for a fast multi-stage charge. Reversible component of heat has been calculated by means of Equation 5. Thermal coefficient dE/dT has been obtained from reference [15]. It can be observed that reversible component of heat corresponds to an endothermic reaction (heat is absorbed) at the beginning of discharge at 4C, but it corresponds to an exothermic reaction (heat is released) when SOC is lower than 40%. When the charge begins at 4C, the reversible component of heat corresponds to an endothermic reaction. The reversible absorbed heat at the beginning of the charge at 4C is equal in magnitude to the reversible released heat at the end of discharge at 4C. Also for charge, when SOC is greater than 40% reactions become exothermic and reversible component of heat is released. The reversible released heat during the end charge is lower than the reversible absorbed heat during the initial discharge due to the 1C-CV charging stages. These reversible components of heat present variations related to staying compounds of graphite [26]. Although at low C rates (< 1C) the reversible components of heat have a considerable weight [27], it can be observed in Figures 3a and 3b that the type Joule (α I^2) irreversible components dominate the total heat generation due to the high rates (4C) used in this work. For this reason, the beginning of the 1C charge stage, see Figure 3b, is crucial to reduce the cell overheating. Heat generation of discharge at 4C interpolates well between the values of reference [16] for discharges at 3C and 6C for the same cell.

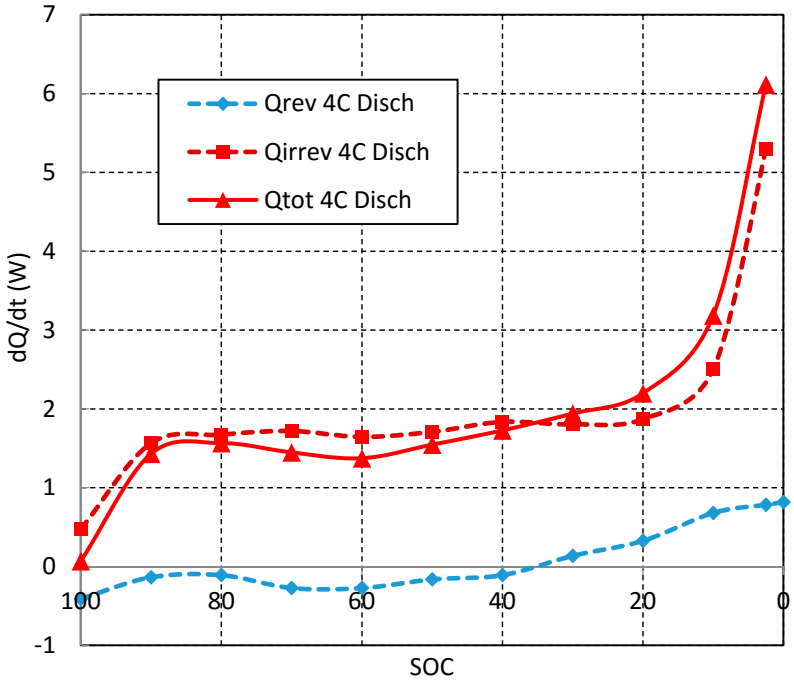

(**a**)

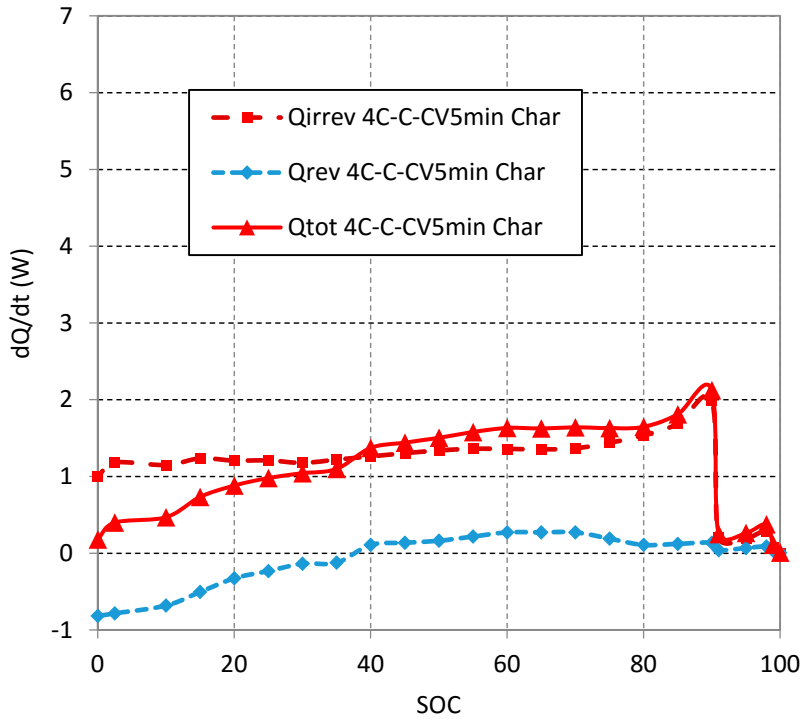

(**b**)

Figure 3. (**a**) Reversible component of heat, irreversible component of heat and total heat evolution profile versus state of charge of the cell, 4C discharge; (**b**) 4C-1C-CV5min charge.

Correlation between the total heat generation, the heat exchange with the environment and temperature variations can be seen in Figure 4a for the 4C discharge and in Figure 4b for the 4C-1C-CV fast charge. For discharge, there is an initial cooling followed by an approximately linear heating for both temperature and heat generation, more noticeable in the area where SOC ranges from 60% to 20%. Below 20% of SOC the heat generation increases faster due to the high value of R_{cell} shown in Figure 2a, but the temperature continues to increase linearly. This fact implies the possibility of a delay cause-effect unidentified, an overestimation of the cell resistance or a very effective evacuation of heat to the outside. The decrease of the temperature at the start of the charge, see Figure 4b, is induced by the resting period of 2 minutes between charge and discharge (not represented), a moderate heat generation due to the endothermic effect shown in Figure 3b and the progressive cooling to the outside.

For charge, the heat generation reaches the maximum when SOC is 90%, at the end of the 4C charge stage. It can be observed that cell temperature and heat dissipation is drastically reduced when the 1C charge stage begins.

Peer-reviewed version available at Batteries 2016, 2, 32; doi:10.3390/batteries2040032

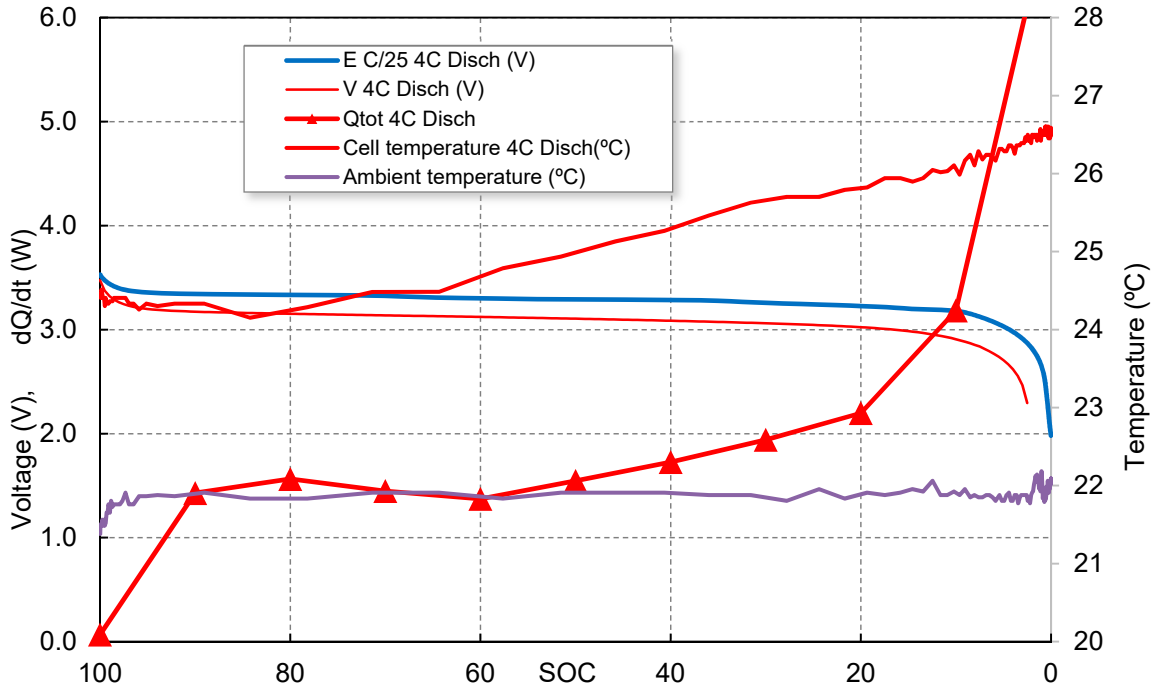

(**a**)

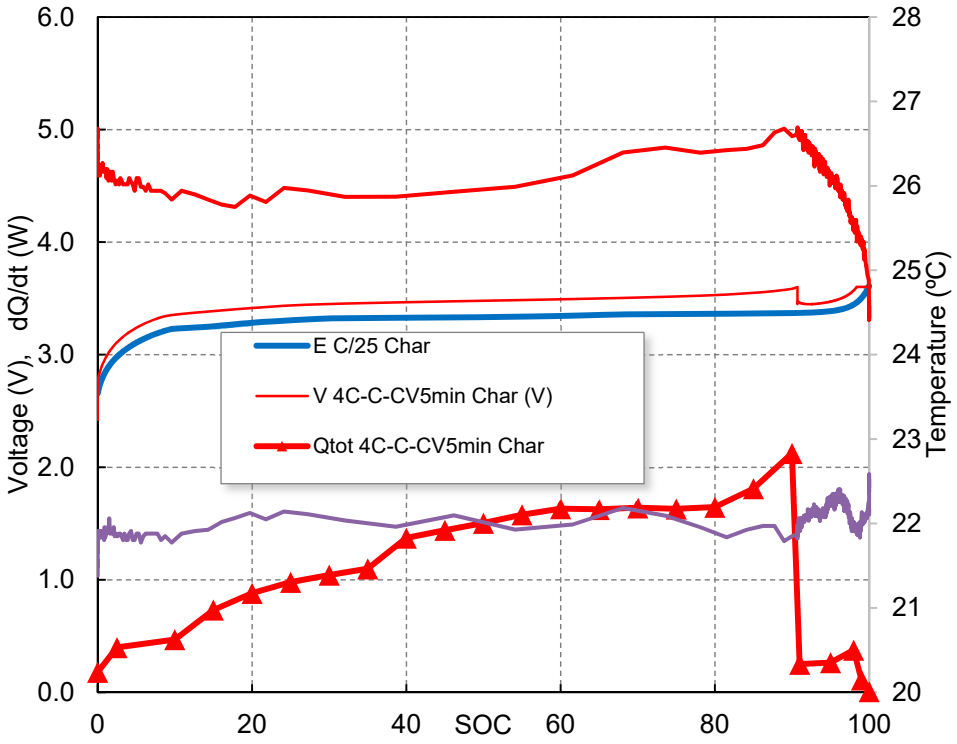

(**b**)

Figure 4. (**a**) Voltages, case temperature and total heat evolution profile versus state of charge of the cell, 4C discharge; (**b**) 4C-1C-CV5min charge.

Peer-reviewed version available at Batteries 2016, 2, 32; doi:10.3390/batteries2040032

Reversible heat generation has not been directly measured in this work but has been estimated from values of dE/dT extracted from [15]. There is also uncertainty in the assessment of SOC scale, related to the fact that discharge at 4C does not end with a CV stage and there is no guarantee that cell charge begins a SOC=0% for all the charging cycles. For these reasons, it has made a partial adjustment of the experimental data to the thermal model. Current is zero and there is no heat generation during the resting period, 2 minutes, between the end of the discharge at 4C and the beginning of the charge at 4C, see Figure 1. Equation 8 becomes Equation 10:

$$\tau_{\text{th}} \frac{dT}{dt} = T_{\text{ext}} - T \quad ; \quad \tau_{\text{th}} = C_{\text{cell}} R_{\text{th}} \tag{10}$$

which is a first order differential equation with a time constant τ_{th}.

The integration of Equation 10 and the adjustment of the experimental data corresponding to the resting period provides $\tau_{\text{th}} = 940$ s.

The average thermal capacity (J/K) of the cell (C/LFP, 2.3 Ah) can be determined by means of the Equation 11 [28]:

$$C_{\text{cell}} = w_{\text{cell}} \times \frac{\sum_i \rho_i c_{\text{P},i} L_i}{\sum_i \rho_i L_i} \tag{11}$$

and data from Table 1. Thickness, L_i, of cell materials have been obtained by dismantling the cell and measuring. Densities (ρ_i) and specific heats ($C_{\text{P},i}$) have been taken from reference [16]. Cell mass was $w_{\text{cell}} = 0.075$ kg. The result for the thermal capacity is $C_{\text{cell}} = 75.6$ J/K, is in accordance with the value of 75.56 J/K of the reference [15], which was measured by means of a direct adjustment of the temperature-time data in the transient area of a thermal cycle once the thermal resistances were measured in stationary state.

Table 1. Several properties of C/LFP 2.3Ah materials.

	Cu	Graphite	Separator	LFP	Al
Thickness (μm)	10	34	16	70	29
Density (Kg m^{-3})	8900	1347.3	1008.9	1500	2700
Specific heat ($JKg^{-1}K^{-1}$)	385	1473.4	1978.2	1260.2	903

The total thermal resistance (internal and external) can be determined by means of the time constant of Equation 10. It has been obtained that $R_{th} = \tau_{th} / C_{cell}$ = (940 s)/(75.6 K) = 12.4 K/W. This value is also identical to that obtained by [15].

5. Conclusions

A study of the thermal behavior of a previous fast charge protocol developed by authors have been made. The casing-time pattern of the temperature during cycling have been qualitatively explained by means of a simple thermal model. This model assumes a uniform internal temperature in the cell. Data from the resting period of the protocol between charge and discharge has been used to adjust the model. Thickness of cell materials measured by authors and thermal properties of the cell materials obtained from literature have been used to determine the thermal parameters of the model: thermal capacity and thermal resistance. For both parameters, the obtained values fully agree with published values that has been obtained with other methodology. This fact supports the use of the simple thermal model. For future works a non-linear adjustment of the whole temperature profile will be carried out. This adjustment will allow the two compounds of thermal resistance to disaggregate.

Acknowledgements

This study was funded in part by the Spanish Ministry of Science and Innovation under Grant DPI2013-46541-R and by the Principality of Asturias Government under Project FC-15-GRUPIN14-073.

References

1. J. Chen, F. Yang, C. Lai, Y. Hwang, R. Lee, A. Abstract, and L. Ion, "A High-Efficiency Multimode Li – Ion Battery Charger With Variable Current Source and Controlling Previous-Stage Supply Voltage," no. July, pp. 2469–2478, 2009.

2. J. S. Neubauer and E. Wood, "Will Your Battery Survive a World With Fast Chargers℗?," *SAE Int*, no. April 2015, pp. 21–23.

3. B. Dunn, H. Kamath, and J.-M. Tarascon, "Electrical energy storage for the grid: a battery of choices.," *Science*, vol. 334, no. 6058, pp. 928–35, Nov. 2011.

4. J. Vetter, P. Novák, M. R. Wagner, C. Veit, K.-C. Möller, J. O. Besenhard, M. Winter, M. Wohlfahrt-Mehrens, C. Vogler, and a. Hammouche, "Ageing mechanisms in lithium-ion batteries," *J. Power Sources*, vol. 147, no. 1–2, pp. 269–281, Sep. 2005.

5. J. Zhang, L. Su, Z. Li, Y. Sun, and N. Wu, "The Evolution of Lithium-Ion Cell Thermal Safety with Aging Examined in a Battery Testing Calorimeter," pp. 1–9, 2016.

6. P. Braun, J. Cho, J. Pikul, W. King, and H. Zhang, "High power rechargeable batteries," *Curr. Opin. Solid …*, vol. 16, pp. 186–198, 2012.

7. Z. Guo, B. Y. Liaw, X. Qiu, L. Gao, and C. Zhang, "Optimal charging method for lithium ion batteries using a universal voltage protocol accommodating aging," *J. Power Sources*, vol.

274, pp. 957–964, Jan. 2015.

8. P. H. L. Notten, J. H. G. O. H. Veld, and J. R. G. Van Beek, "Boostcharging Li-ion batteries: A challenging new charging concept," *J. Power Sources*, vol. 145, no. 1, pp. 89–94, Jul. 2005.

9. A. Khandelwal, K. S. Hariharan, P. Gambhire, S. M. Kolake, T. Yeo, and S. Doo, "Thermally coupled moving boundary model for charge e discharge of," *J. Power Sources*, vol. 279, pp. 180–196, 2015.

10. D. Anseán, M. González, J. C. Viera, V. M. García, C. Blanco, and M. Valledor, "Fast charging technique for high power lithium iron phosphate batteries: A cycle life analysis," *J. Power Sources*, vol. 239, pp. 9–15, 2013.

11. D. Anseán, M. Dubarry, A. Devie, B. Y. Liaw, V. M. García, J. C. Viera, and D. Anse, "Fast charging technique for high power LiFePO 4 batteries◎: A mechanistic analysis of aging," *J. Power Sources*, vol. 321, pp. 201–209, 2016.

12. C. R. Pals and J. Newman, "Thermal Modeling of the Lithium / Polymer Battery," *J. Electrochem. Soc.*, no. October, pp. 1–8, 1995.

13. K. Onda, T. Ohshima, M. Nakayama, K. Fukuda, and T. Araki, "Thermal behavior of small lithium-ion battery during rapid charge and discharge cycles," *J. Power Sources*, vol. 158, no. 1, pp. 535–542, Jul. 2006.

14. Y. Inui, Y. Kobayashi, Y. Watanabe, Y. Watase, and Y. Kitamura, "Simulation of temperature distribution in cylindrical and prismatic lithium ion secondary batteries," *Energy Convers. Manag.*, vol. 48, no. 7, pp. 2103–2109, Jul. 2007.

15. C. Forgez, D. Vinh, G. Friedrich, M. Morcrette, and C. Delacourt, "Thermal modeling of a cylindrical LiFePO 4 / graphite lithium-ion battery," vol. 195, pp. 2961–2968, 2010.

16. Y. Ye, L. H. Saw, Y. Shi, K. Somasundaram, and A. A. O. Tay, "Effect of thermal contact resistances on fast charging of large format lithium ion batteries," *Electrochim. Acta*, vol. 134, pp. 327–337, 2014.

17. D. Anseán, V. M. García, M. González, J. C. Viera, J. C. Antón, and C. Blanco, "Evaluation of LiFePO4 batteries for Electric Vehicle applications," *IEEE Trans. Ind. Appl.*, vol. 51, no. 2, pp. 1855–1863, 2015.

18. "USAB Consortium ELECTRIC VEHICLE BATTERY TEST PROCEDURES Revision 2," no. January 1996. p. 129, 1996.

19. M. Dubarry and B. Y. Liaw, "Identify capacity fading mechanism in a commercial LiFePO4 cell," *J. Power Sources*, vol. 194, no. 1, pp. 541–549, Oct. 2009.

20. I. Bloom, S. A. Jones, E. G. Polzin, V. S. Battaglia, G. L. Henriksen, C. G. Motloch, R. B. Wright, R. G. Jungst, H. L. Case, and D. H. Doughty, "Mechanisms of impedance rise in

326 high-power, lithium-ion cells," *J. Power Sources*, vol. 111, pp. 152–159, 2002.

327 21. M. Dubarry, C. Truchot, and B. Y. Liaw, "Synthesize battery degradation modes via a
328 diagnostic and prognostic model," *J. Power Sources*, vol. 219, pp. 204–216, 2012.

329 22. J. Dahn, "Phase diagram of LixC6.," *Phys. Rev. B. Condens. Matter*, vol. 44, no. 17, pp.
330 9170–9177, Nov. 1991.

331 23. W. Dreyer, J. Jamnik, C. Guhlke, R. Huth, J. Moskon, and M. Gaberscek, "The
332 thermodynamic origin of hysteresis in insertion batteries.," *Nat. Mater.*, vol. 9, no. 5, pp. 448–
333 53, May 2010.

334 24. M. A. Roscher, J. Vetter, and D. U. Sauer, "Characterisation of charge and discharge
335 behaviour of lithium ion batteries with olivine based cathode active material," *J. Power*
336 *Sources*, vol. 191, no. 2, pp. 582–590, Jun. 2009.

337 25. D. Anseán, V. M. García, M. González, J. C. Viera, C. Blanco, and J. L. Antuña, "DC
338 internal resistance during charge◉: analysis and study on LiFePO 4 batteries," *Electr. Veh.*
339 *Symp. EVS27. Barcelona, Nov. 2013*, pp. 1–11, 2013.

340 26. Y. Reynier, R. Yazami, and B. Fultz, "The entropy and enthalpy of lithium intercalation
341 into graphite," *J. Power Sources*, vol. 119–121, pp. 850–855, Jun. 2003.

342 27. A. Khandelwal, K. S. Hariharan, V. Senthil Kumar, P. Gambhire, S. M. Kolake, D. Oh,
343 and S. Doo, "Generalized moving boundary model for charge–discharge of LiFePO4/C
344 cells," *J. Power Sources*, vol. 248, pp. 101–114, Feb. 2014.

345 28. S. C. Chen, C. C. Wan, and Y. Y. Wang, "Thermal analysis of lithium-ion batteries," *J.*
346 *Power Sources*, vol. 140, no. 1, pp. 111–124, Jan. 2005.

347

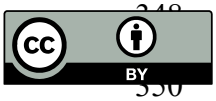

351